Nuclear Instruments and Methods in Physics Research A272 (1988) 800–813
North-Holland, Amsterdam

PROPORTIONAL COUNTERS AS LOW ENERGY PHOTON DETECTORS

Keith JAHODA * and Dan McCAMMON

Physics Department, University of Wisconsin, Madison, Wisconsin 53706, USA

Received 12 May 1987 and in revised form 12 February 1988

We have investigated the response of an argon–methane proportional counter to monochromatic X-rays in the range 99–277 eV. The apparent nonlinearities in mean pulse height as a function of photon energy and the detailed shape of the pulse height distribution for each energy can be predicted quite precisely using the extensive atomic data available for argon. Based on this understanding, we propose a semiempirical system for using a limited amount of calibration data to predict the full response of counters employing less well characterized gasses.

Such accurate models of proportional counter response are required to maximize the spectral information that can be derived from observed pulse height distributions.

1. Introduction

Gas filled proportional counters have a long history as detectors for low energy X-rays. Although solid state detectors and microchannel arrays have supplanted them for certain applications, they retain distinct advantages for many others. Among these are:

(a) High efficiency: Peak quantum efficiencies can be above 90%.

(b) Wide bandwidth: It is possible to design a single detector with quantum efficiency above 30% over two decades in photon energy.

(c) Large area: Proportional counters can be scaled to almost arbitrarily large sizes with low weight and cost relative to other detectors.

(d) Low background: Background rates less than 2×10^{-4} counts cm^{-2} s^{-1} keV^{-1} down to 70 eV have been observed for counters exposed to the cosmic ray flux above the atmosphere. Much lower rates are possible at energies where a front-side anticoincidence layer can be used.

(e) Position resolution: Counters can be constructed to provide one or two dimensional imaging capability with better than 300 μm resolution.

(f) Energy resolution: Proportional counters are the only detectors now in use with any energy resolution at all for photon energies below the amplifier noise limit of small Si(Li) detectors – currently ~ 200 eV. Even the very low resolving power available in this region ($E/\Delta E \sim 1$) can be invaluable for discriminating against non-X-ray background and other interference, such as overlapping orders in a grating spectrometer.

All of the above characteristics are vital for some aspects of X-ray astronomy; in various combinations, they make proportional counters highly attractive for many other applications.

The limited energy resolution of proportional counters requires an indirect method for analysis of almost any spectrum more complicated than a single line. The usual procedure is to assume a trial input spectrum, calculate the expected response of the detector to this spectrum using a model of the counter response, compare this predicted pulse height spectrum with the observed data, and modify the trial spectrum. This process is iterated until a good match is obtained. A considerable amount of spectral information can be derived in this way if the pulse height data have good statistical precision, but an accurate model of the proportional counter response is required.

The usual method for determining the response model is to measure the pulse height distributions obtained from a small number of X-ray fluorescent lines of known energy, and to fit them to a predetermined function with adjustable mean and shape parameters. The adjustable parameters are then interpolated to find the appropriate values for all other photon energies. Functions typically used are Poisson distributions, Prescott functions [1], and, at energies above a few keV, Gaussians. Since there is some evidence that for low photon energies neither the mean pulse height nor the shape of the distribution is adequately predicted by such procedures, we have used a synchrotron radiation source with a high-resolution monochromator to measure the detailed response of an argon–methane filled proportional counter to X-rays with energies between 99 and 277 eV.

Fig. 1 is a plot of the means from Poisson fits to the

* Present address: Code 666, NASA/Goddard Space Flight Center, Greenbelt, Maryland 20771, USA.

0168-9002/88/$03.50

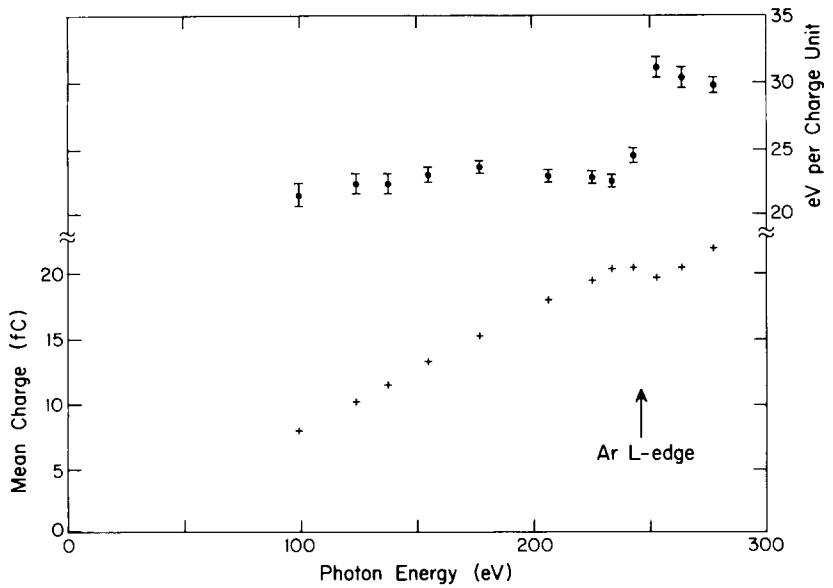

Fig. 1. The mean charge (crosses) and the width parameter (dots) determined by fitting Poisson distributions to the pulse height spectra generated by monoenergetic X-rays. The uncertainties in the mean charge are comparable to the size of the symbols. The width parameter is in units of eV per charge unit. Both parameters are discontinuous at the argon L-edge.

pulse height spectra. A zero offset and a ~ 12% discontinuity at the argon L-edge (246 eV) are evident. The width parameter, in terms of an apparent eV per charge unit, is shown at the top of the figure and also has a large discontinuity at the argon L-edge. As an example of the quality of the individual fits, fig. 2 shows the difference between the observed pulse height distribution due to 177 eV photons and the best fit Poisson, as well as results for two other models. It can be seen that the Poisson distribution is a poor representation. The Prescott function is better, but still has significant systematic errors in shape. The third model represents our

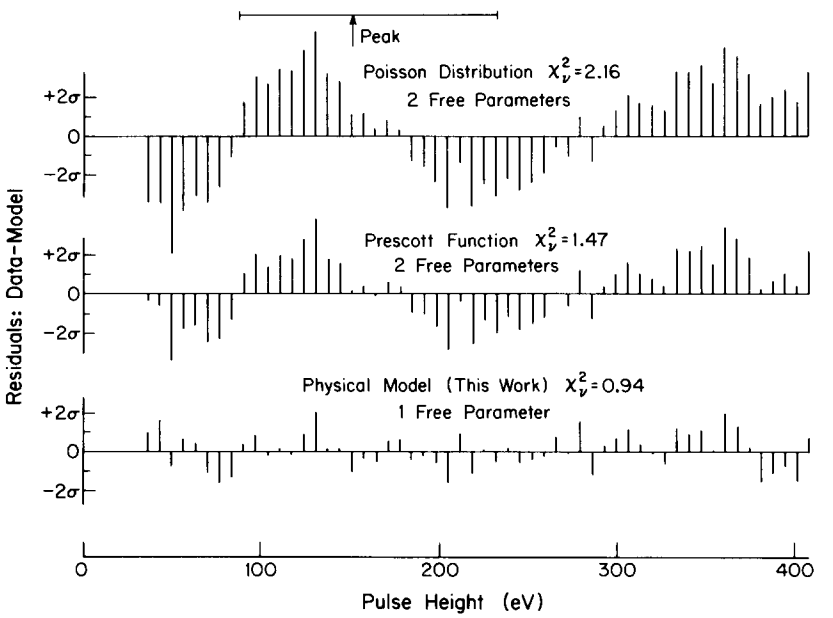

Fig. 2. Residuals for three models of the pulse height distribution produced by 177 eV photons, plotted as data minus model in units of one standard deviation of the data (1.7% at the peak). The position of the peak and the full width at half maximum are indicated at the top of the figure. See section 4 for discussion of the requirement for a free parameter in the physical model.

attempt to improve on this situation by using a less empirical approach. The atomic properties of argon have been particularly well studied, and we have made use of this information to try to calculate the counter response from first principles. We find that we can predict the observed behavior rather accurately: the residuals for the 177 eV pulse height distribution shown in fig. 2 are typical, and the nonlinearities of the mean pulse height with respect to photon energy shown in fig. 1 are also explained.

Unfortunately, physical data similar to those available for argon do not exist for most other gasses. If we assume, however, that the relative importance of the various effects is not too different, we can use our understanding of argon to interpolate the response of counters filled with other gasses between a small number of appropriately chosen calibration lines. A general procedure for doing this is outlined in section 5.

2. Proportional counter operation

Three distinct processes are involved in the conversion of an X-ray photon to the charge output signal of a proportional counter:

(1) photoionization, in which the incident photon energy is converted into electron kinetic energy and residual ionization potential,
(2) secondary ionization, in which the free electrons lose kinetic energy through ionizing and non-ionizing collisions with other gas atoms, and
(3) the electron avalanches, which amplify the signal so that readout noise does not dominate.

2.1. Photoionization

To be recorded by a proportional counter, an X-ray must produce ionization in the active volume of the counter. The only significant interaction for soft X-rays is photoelectric absorption. In the simplest case an outer shell electron is removed, producing a singly ionized atom and a single energetic electron. Inner shell ionization dominates when energetically allowed, however, and usually leaves the absorbing atom in a multiply ionized state due to emission of one or more Auger electrons. In all cases the photon energy is split between the potential energy of the final ion state and the kinetic energy of one or more electrons. Because the ion drifts to the cathode without producing any additional free electrons, its potential energy is effectively lost from the counter. (Ionizing charge exchange collisions are energetically allowed for Ar^{3+} and above, but this does not seem to be a significant effect.)

The deeper the shell from which the initial photoionization occurs, the higher the average ionization state the atom is left in. This means that as the photon energy is increased across an absorption edge and it becomes energetically possible to remove a more tightly bound electron, there will be a sudden decrease in the kinetic energy available to the electrons. This energy loss is partially offset by the extra electrons produced since each free electron, even with zero kinetic energy, represents an amount of energy equal to the average kinetic energy required per secondary ionization in the gas (the "W-value": see section 2.2 below). Additional energy loss occurs due to the "shake-up" and "shake-off" effects where outer shell electrons are left in excited states or are removed from the atom due to perturbations caused by the energetic photoelectron or Auger electrons.

For argon, good data exist for the probabilities and cross sections for almost all of these processes. We have used these to calculate the distribution of numbers of electrons produced in a photoionization event and their kinetic energies. Details of the calculation are published elsewhere [2]. We find that the net increase in energy loss from the electron system on crossing the argon L-edge accounts for about half of the discontinuity in mean pulse height at that point shown in fig. 1. (The other half is caused by losses of part of the secondary electron cloud through diffusion to the window. This loss mechanism is more important on the high-energy side of the edge because of the much smaller photon absorption depth, as discussed in section 2.2. An experiment performed to verify this division of the cause of the discontinuity is described in section 4. The sudden increase in the *width* of the pulse height distribution at the L-edge is primarily due to the effects of diffusion to the window.)

Branching ratios for the more important processes vary only slightly with photon energy between absorption edges. This means that the amount of energy lost to potential energy of the ion is nearly constant between absorption edges, but that there can be a relatively large change in this loss as the photon energy is increased across an absorption edge. This observation is the key to an empirical procedure employing a minimum number of calibration lines to model the response of proportional counters using different gasses: photoionization is the most complex contributor to counter behaviour, but it is usually sufficient to evaluate its effects at one photon energy in each interval between absorption edges.

2.2. Secondary ionization

The ionization yield, $W(E)$, is defined as the initial electron kinetic energy divided by the average number of ionizations, and is in general a function of the initial energy of the electron. For most gasses $W(E)$ approaches a constant value of about 30 eV per ion pair as the initial electron energy exceeds a few hundred eV.

Particularly precise measurements of this function have been made for a number of gasses by Combecher [3]. These data show that $W(E)$ has high values just above the ionization potential and decreases rather smoothly, approaching a limiting value at energies above several hundred eV. It turns out that this variation can be fit almost perfectly with a simple offset, as shown in fig. 3 where Combecher's data have been plotted as the mean number of electrons produced vs the initial energy. The initial electron has been included in the total since it is indistinguishable from the others once thermalization is complete. The solid line on the figure is an extrapolation to low energies of a least-squares fit to the data between 200 and 500 eV for the function

$$N_{\mathrm{tot}} = (E - U)/W + 1 \quad \text{for} \quad E > 15.8 \text{ eV},$$
$$= 1 \quad \text{for} \quad E < 15.8 \text{ eV}. \qquad (1)$$

The fit values are 10.6 eV for the offset U, and 28.5 eV for the reciprocal slope W. The latter is, of course, equal to the high energy limiting value of $W(E)$. ($W(E)$ decreases slightly at much higher energies, but this is not of interest here.)

The accuracy of the linear approximation is remarkable, considering the complexity of the physics involved in $W(E)$. Conservation of energy requires $N_{\mathrm{tot}} = 1$ for E less than the ionization potential of argon, and for E only 2 eV above this level, the average yield is already within 2% of the straight line approximation. Fits to Combecher's data for other gasses give similar results. Methane in particular has parameters quite close to argon, with $W = 28.6$ eV, $U = 11.0$ eV, and an ionization potential of 12.6 eV. The shape of N_{tot} vs E observed for these gasses is in good qualitative agreement with theoretical estimates [4].

Since $W(E)$ is greater than the ionization potential, the initial electron kinetic energy must be distributed between ionizing and non-ionizing processes, and statistical fluctuations in the branching ratio produce a distribution in the actual number of ionizations produced by electrons with a given kinetic energy. The second moment of this distribution is described by the Fano factor, f, where $\sigma^2 = f\langle N \rangle$. Here, σ^2 is the variance, and $\langle N \rangle$ is the average number of secondary ionizations, $N_{\mathrm{tot}} - 1$. The Fano factor has been calculated for some gasses. In argon, for instance, Alkhazov [5] predicts 0.16 using analytical approximations, and Unnikrishnan and Prasad [6] calculate 0.15 for $E > 300$ eV using a Monte Carlo technique. These can be compared with the value of 0.18 measured at 5.3 MeV [7].

The full shape of the distribution is obtained from the Monte Carlo calculations. We find that Unnikrishnan and Prasad's data can be approximated to a few percent precision by a Gaussian truncated at zero and evaluated for integer numbers of electrons [8].

Some of the secondary electrons may not reach the avalanche region. An important loss mechanism at some X-ray energies is the loss of secondary electrons by diffusion back to the counter window. This depends on a competition between diffusion rate and drift velocity, and should be significant when the length scale defined by the ratio of diffusion coefficient to electron drift velocity, (D/w), is comparable to the mean photon

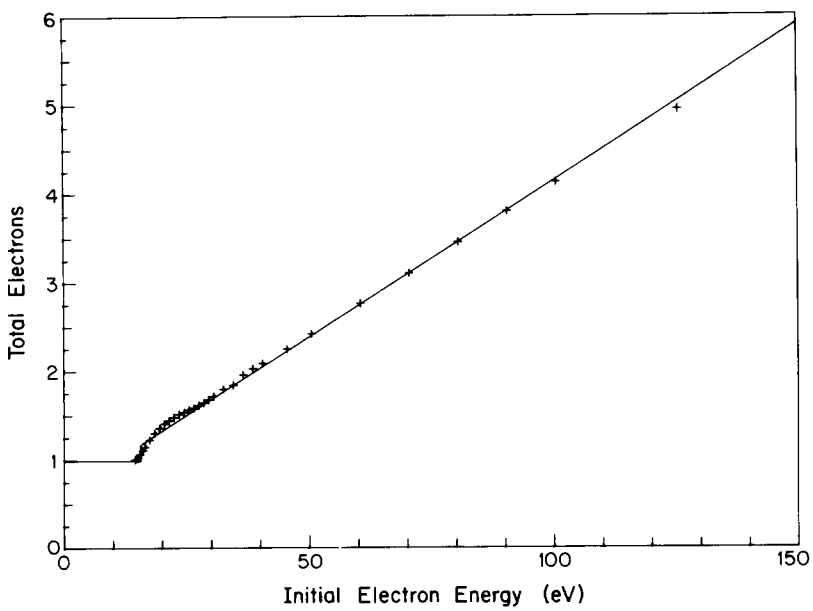

Fig. 3. Total secondary ionization produced by an energetic electron in argon as a function of electron energy. The number includes the original electron. Crosses are experimental data [3]; the line is fit to data for $200 < E_{\mathrm{el}} < 500$ eV.

absorption depth λ. A simple model for this process has been developed by Inoue et al. [9]. They find that diffusion losses are important for $D/w \gtrsim 0.1\lambda$, a condition satisfied for some distance above the argon L-edge in most argon–methane counters. (The possibility of an energetic photoelectron reaching the window before being completely thermalized seems unlikely under any conditions of interest due to the large ratio of photon to electron range at any given energy.) In counters with plane-parallel geometry, the effective transmission of the grid separating the drift and avalanche regions must be taken into account as an additional loss mechanism.

2.3. Electron avalanche

In conventional proportional counters the secondary electrons drift into a region where the electric field is high enough that electrons can gain sufficient energy between collisions to ionize additional gas atoms, forming multiplicative cascades or avalanches. Each secondary electron produces its own avalanche, and the mean number of electrons in one of these is referred to as the "gas gain". This gain is required in order that amplifier noise not dominate the counter resolution.

If the individual ionizing collisions in an avalanche were uncorrelated, we would expect the distribution of total charge collected in single electron avalanches to be an exponential, which has a variance equal to the square of the mean. However, a significant fraction of the energy gained from the field goes into the ionizations, so the individual multiplications are not quite independent events. This anticorrelation reduces the variance. The theoretical work of Alkhazov [10] predicts that the shape of the charge distribution in single-electron avalanches (the single electron spectrum, or SES) should be approximated by a Polya distribution:

$$P(q,\mu,h)=\frac{1}{\mu}\frac{h^h}{\Gamma(h)}\exp\left(\frac{-hq}{\mu}\right)\left(\frac{q}{\mu}\right)^{(h-1)}. \qquad (2)$$

Here q is the actual number of electrons produced in an avalanche, μ its mean value (the "gas gain"), h is a width parameter which we call the Polya parameter, and Γ is the Gamma function. This distribution reduces to an exponential for $h=1$ and approaches a delta function as h becomes large. Measurements of the SES in proportional counters with a cylindrical field geometry generally are in good agreement with this form [11,12]. The values of h are typically between 1.3 and 1.5 and the relative variance, which is just h^{-1}, is between 0.6 and 0.8.

In the normal operation of proportional counters as X-ray detectors the SES is not directly observed, since each X-ray photon produces several electrons which initiate avalanches. The detector output is the sum of the charge produced by these avalanches. The Polya function has the convenient mathematical property that the distribution of sums of N samples from a Polya distribution with mean μ and Polya parameter h is another Polya distribution with mean $N\mu$ and Polya parameter Nh. This gives the relative variance in the distribution of total charge produced by exactly N secondary electrons as $(Nh)^{-1}$.

We can compare this relative variance in the total avalanche charge to the relative variance in the number of secondary electrons produced by monoenergetic electrons in a gas, which was defined in section 2.2 to be $f\langle N\rangle^{-1}$, where $\langle N\rangle$ is the mean number of secondaries produced and f is the Fano factor for the gas. Since f is typically ~ 0.2 and h^{-1} is ~ 0.7, it is clear that avalanche fluctuations strongly dominate secondary ionization statistics in determining proportional counter resolution.

The assumption of a Polya distribution for the SES may be less accurate for counters with plane parallel rather than cylindrical field geometries [10]. The apparent SES can also be distorted by successor avalanches, which are initiated by photoelectrons liberated from the detector cathode by ultraviolet photons produced in the original avalanche. These can greatly increase the variance of the SES, but are usually a problem only when using a cathode material with a high photoelectric efficiency or a counter gas which is particularly transparent to ultraviolet photons. The successor avalanches primarily affect the high-charge tail of the SES where the resulting distortions can be observed directly; they can also be resolved in time with sufficiently fast electronics [13].

Recently, at least three new varieties of proportional counters have been developed to take advantage of the large improvement in resolution which can be obtained by reducing the effect of avalanche fluctuations. The first of these, the gas scintillation proportional counter, eliminates the avalanche entirely, using instead a lower-field region to produce a large number of ultraviolet photons from each secondary electron in a non-multiplicative process [14]. The total light output then provides an estimate of the number of secondary electrons. The second variety of counter retains the avalanche region, but uses fast electronics to resolve in time the individual avalanches produced by each secondary electron. The sizes of the avalanches are ignored, and only the number is recorded [15]. The third still uses total avalanche charge as the signal, but employs a Penning gas mixture and an optimized field in the avalanche region to greatly increase the ionization efficiency. The increased efficiency reduces the variance by increasing the anticorrelation between ionizing events [10,16,17]. While some avalanche fluctuation effects still exist, Penning mixtures generally have exceptionally small Fano factors, and the net resolution is in principle at least as good as for the other two counters. In

practice, all three of these schemes have demonstrated about a factor of two improvement in resolution over conventional proportional counters. The effects of photoionization and secondary ionization statistics on detector response still apply to these counters. More accuracy may be required in calculating the photoionization effects since avalanche fluctuations will no longer dominate the shape of the final pulse height distribution.

A few other well-known effects exist which are hardly fundamental but which must be taken into account for many detectors. These are positional nonuniformities, gain saturation nonlinearity, and rate-gain effects. The first is usually due to changes in the field geometry of the avalanche region from one point on the counter to another. It can be evaluated empirically with an adequate amount of counter mapping data. The last two are caused by a breakdown of the assumption of independence of the single electron avalanches due to field reductions in the avalanche region produced by ions left by other avalanches. In the case of gain saturation nonlinearity, the other avalanches are part of the same X-ray event, and the effect becomes more pronounced as the X-ray energy increases since a higher density of avalanches is produced. For rate-gain effects, the interfering ions are left from previous X-ray events, and the effect is more serious at high counting rates. These effects are smoothly varying functions of X-ray energy and counting rate, respectively, and are easily calibrated with a few data points as long as the gain reductions are small. If large effects occur at photon energies or counting rates of interest, it is best to reduce the gas gain to make the detector better behaved.

3. Outline of the model calculations

For argon, the basic data governing all the processes described in section 2 can be found in the literature. In addition, detailed calculations using these data are available for the distribution of secondary electrons produced by thermalization of an energetic electron, and for the distribution of final sizes of avalanches induced by a single electron in a given field geometry and gas density. We have collected all of this information into a model of the overall response of a cylindrical argon–methane counter to monoenergetic photons. The details of this procedure and the sources of the data used are given in Jahoda and McCammon [2]; we summarize the method and present the results here.

The photoionization process can take any of a number of different branches, starting with the atomic shell initially photoionized, the number of Auger electrons ejected, and the possible bound or free states to which other electrons can be promoted by "shake-up" or "shake-off". For each allowed combination, we calculate the net probability and produce a list of free electrons released in the gas with their individual kinetic energies.

Electrons with energies less than the ionization potential of the gas can produce no further ionization and are retained as single electrons. Each of the more energetic electrons will produce a distribution of additional electrons by collisional ionization. The means and shapes of these distributions are calculated for the initial kinetic energy, and the individual distributions are convolved and the single electrons added in to give a net distribution of thermal electrons for this particular branch. This procedure is repeated for each allowed branch, and the branch distributions are weighted by their respective branch probabilities and summed to give an overall distribution of numbers of secondary electrons produced by a particular photon energy. The distribution of losses through diffusion back to the counter window is then calculated and convolved with this to derive the distribution $Q(i)$ for the probability Q that exactly i electrons will reach the avalanche region.

Following results from the literature, the distribution of collected charge q from an avalanche initiated by a single electron is assumed to be given by the Polya function $P(q, \mu, h)$ (eq. (2)). Here μ is the mean effective charge produced, which is just the apparent gas gain, and h is a width parameter whose value depends only on the electric field and gas density in the avalanche region. (The apparent gas gain differs from the true gas gain because charge amplifiers do not usually integrate for the full length of time required for the positive ions to reach the cathode.) Due to the properties of the Polya function, the distribution of total charge q collected from exactly i avalanches is $P(q, i\mu, ih)$. The net pulse height distribution produced by monoenergetic photons is then given by the weighted sum:

$$R(q) = \sum_i (Q(i) P(q, i\mu, ih)). \tag{3}$$

Fig. 4 shows the relative effects of these different processes for 277 eV photons. To display the magnitude of the effects of branching in the photoionization stage, the *mean* number of electrons produced by each energetic electron in a given branch was calculated. These were summed together with individual electrons to give the mean total number of electrons produced by that branch. The solid triangles are the branch probabilities plotted at their respective mean numbers, and, aside from the fractional electrons, this represents the distribution of secondary electrons that would be expected from photoionization branching in the absence of statistical fluctuations in the secondary ionization process (Fano factor = 0). The open histogram shows the actual distribution of secondary electrons produced, and has the same mean as the triangles. The solid histogram is the distribution $Q(i)$ after diffusion losses to the window

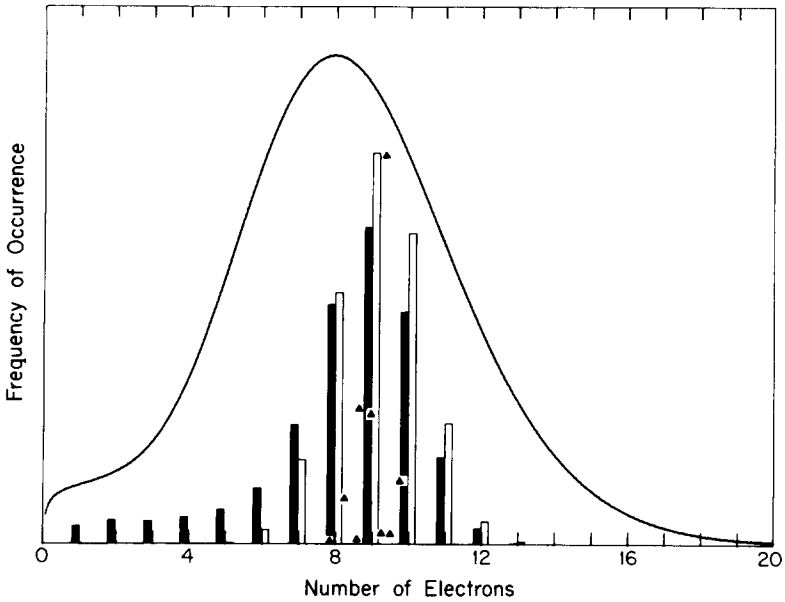

Fig. 4. Contributions of various processes to broadening of the proportional counter pulse height spectrum. The triangles show the distribution of mean numbers of secondary electrons that would be produced following absorption of a 277 eV photon if there were no statistical fluctuations associated with the secondary ionization. Each triangle represents a different branch of the photoionization process. The open histogram shows this distribution when the effects of secondary ionization statistics are included. The shaded histogram is the same distribution after diffusion losses to the window. The solid line shows the detector output after avalanche statistics are included.

are included. The solid line is the distribution of total avalanche charge $R(q)$, plotted in units of the apparent gas gain μ so that it has the same mean as the solid histogram. The secondary electron distribution is largely obscured by statistical fluctuations in the avalanche process and the experimental comparisons with our data (section 4) are not very sensitive to this part of the model. We can, however, compare our predictions of the secondary electron distribution to the data of Siegmund et al. [15], who used high-speed electronics to count flashes of light from the individual avalanches induced by each secondary electron. They determined the number of avalanches associated with each X-ray absorbed in their counter and thus measured directly the distribution of numbers of secondary electrons. The distribution presented by Siegmund et al. for 277 eV carbon K_α photons in an argon filled counter is continuous, rather than a histogram, due to the 0.7 electron (1σ) noise introduced by the count summing circuit. The dots in fig. 5 show their measured avalanche count distribution for C K_α photons while the histogram is our calculated secondary electron distribution for 277 eV photons. The solid line shows the histogram after convolution with a Gaussian ($1\sigma = 0.7$ electrons) to facilitate comparison. (Siegmund et al. used a somewhat different gas mixture and drift field than those in our calculations so the diffusion losses to the window may be somewhat different [2].) The sharp rise at small electron numbers in the Siegmund et al. data is probably due to noise in the count summing circuit. The overall agreement between the distributions is quite

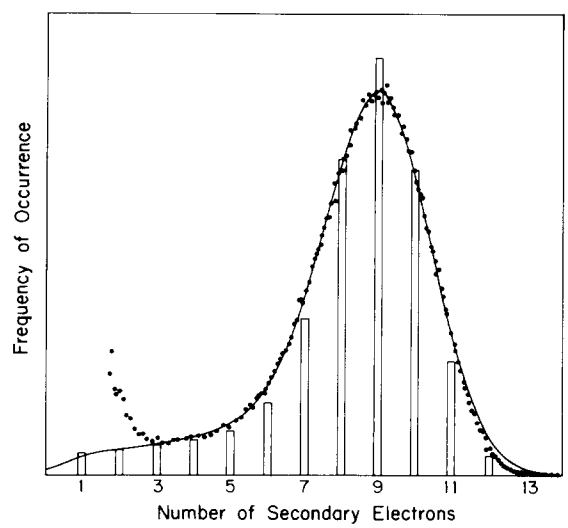

Fig. 5. A comparison of the secondary electron distribution for monochromatic 277 eV X-rays calculated from the detailed model (histogram) with the direct measurement of Siegmund et al. [15] (points). The solid line shows the model distribution convolved with a Gaussian of width equal to the electronic noise in the summing circuit used to take the data.

reasonable, and adds credibility to the calculations in our model up to this point.

It can be seen from fig. 4 that photoionization branching contributes little to the width of the final pulse height distribution. There is almost no change in the branching pattern in the energy interval between atomic absorption edges, and the mean number of secondaries varies quite linearly with photon energy except for a small energy range immediately above an edge. These observations are significant for empirical models fit to limited amounts of calibration data: since the photoionization effects are the most complex part of the proportional counter behavior, it is fortunate that their effect on the shape of the response does not have to be taken into account in any detail. There can be a large shift in the average number of secondaries across an absorption edge, primarily due to a shift in the mean final ionization state of the absorbing atom, but this can be evaluated by having at least one calibration line located somewhat within each energy interval between successive absorption edges.

4. Comparison of model with experiment

We have used a synchrotron light source and a double grating monochromator with particularly low scattered light levels to generate the pulse height spectra of monochromatic photons at twelve energies from 99 to 277 eV. Our gas proportional counter was filled with P-10 (90% argon, 10% methane) at a pressure of 780 Torr. The apparent gas gain was about 1.6×10^4 as determined by measurements with an ^{55}Fe source and a charge pulser in the usual manner. The true gain (from total current measurements) was about twice this value. Slow gain variations over the course of the experiment were monitored by measuring the peak position of the ^{55}Fe pulse height spectrum. The gain variations were less than 3% and have been corrected with an accuracy of about 1%.

The data are displayed in fig. 6. The photon energy which generated each pulse height distribution is indicated in the figure. The measured pulse height spectra with $E \leqq 142$ eV were contaminated by a significant amount of second order flux from the monochromator. For these three pulse height spectra we used the model to calculate the shape and position of the second order line, and fit its amplitude as an additional free parameter. This second order contribution, which accounted for about 25% of the observed X-rays in the 99 eV pulse height distribution, has been removed from the data displayed in the figure.

The results of the models discussed above and described in detail in Jahoda and McCammon [2] are shown as solid lines in fig. 6. A measured background spectrum has been added to the models. The fits to the

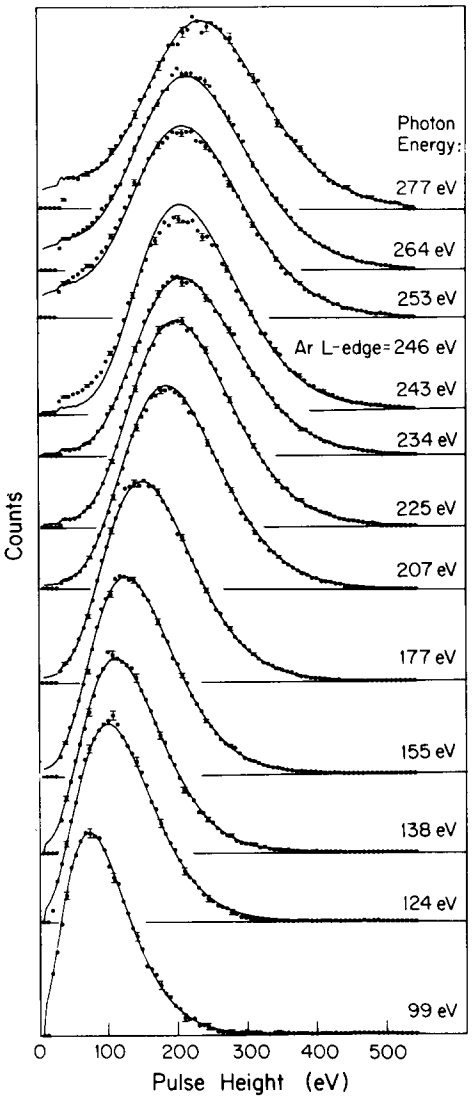

Fig. 6. Pulse height spectra produced by monoenergetic photons in an argon–methane proportional counter. The photon energies are indicated on the figure, as is the location of the argon L-edge. Models of the counter response are shown as solid lines. Counter gas gain is the only free parameter in these models.

pulse height spectra produced by photons at 243 and 253 eV (just below and above the argon L-edge) are poor. This could be due to wings on the monochromator line profile which extend across the edge or to fine structure near the atomic absorption edge which is unaccounted for in the model. Because of the ~1% uncertainty in the experimental gain normalization and the high statistical precision of the data, it was necessary to allow the gas gain to vary as a free parameter. All other aspects of the model, i.e. the details of the photoionization process, the secondary electron yield

and the distribution of the secondary electrons, diffusion losses to the window, and the shape of the avalanche distribution, are fixed by data obtained from the literature. Values of the reduced chi-square, χ^2_ν, for each pulse height spectrum are listed in column 2 of table 1.

As a sensitive test of the effectiveness of this model in explaining the discontinuities in the mean and width of the observed pulse height distributions across the argon L-edge shown in fig. 1, we ran another series of fits where both the gain and the basic width parameter (the single electron Polya parameter, h) were allowed to vary freely. In figs. 7a and 7b we plot the gas gain and width parameter derived from these fits. The fit values for gas gain are almost identical to the values obtained with h fixed at 1.41. The χ^2_ν values for these fits are listed in column 3 of table 1. The gas gain shows no consistent trend with photon energy, and in particular there is no significant shift across the argon L-edge. The

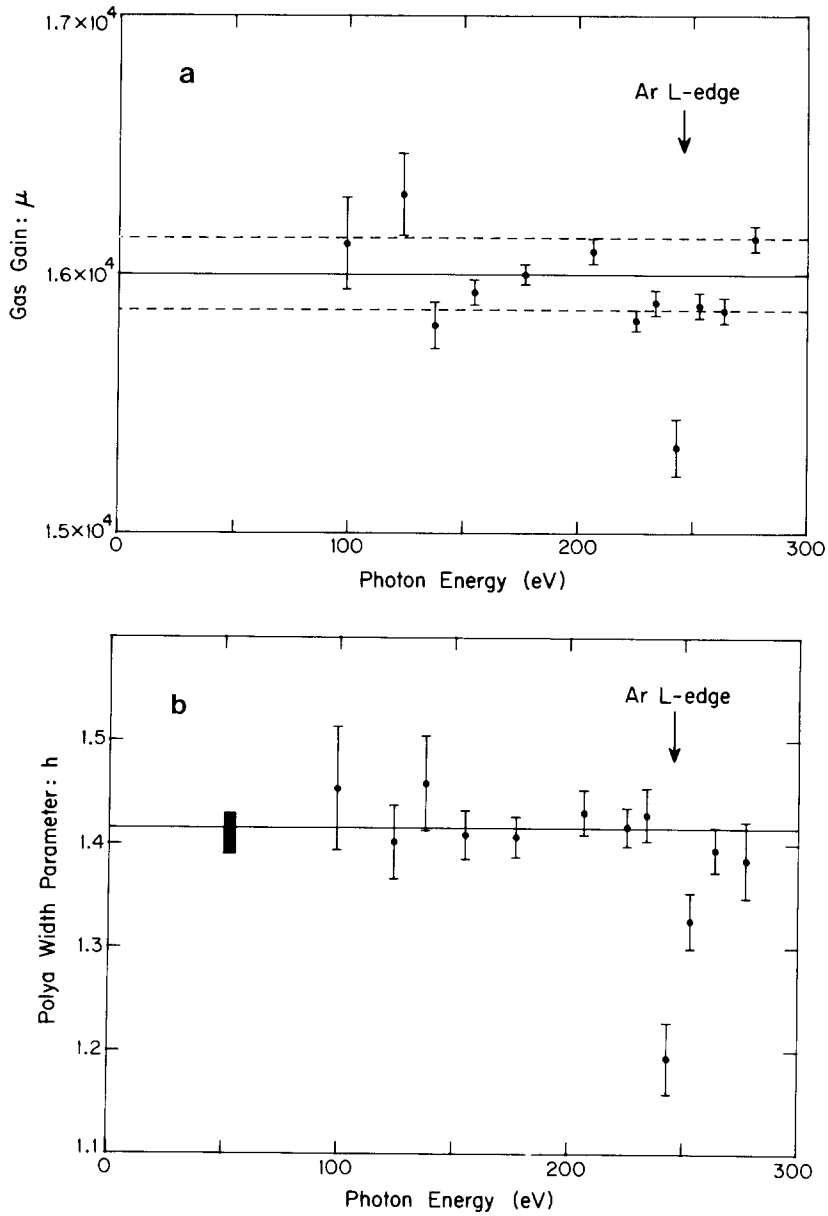

Fig. 7. Best fit values of the gas gain μ (a) and the single electron spectrum width parameter h (b) for models which treated both as free parameters. The horizontal lines in (a) show the mean gain to which the spectra were reduced using a ^{55}Fe calibration source and the $\pm 1\%$ estimated uncertainty in this procedure. The vertical bar in (b) indicates the uncertainty in the value of h derived from the literature [18]. The solid line is the average of the fitted values.

Table 1
Summary of model fitting results

E_γ [eV]	Reduced chi-square, χ^2_ν			
	Physical models [a]		Semiempirical	
	h fixed at 1.41	h, μ free parameters	$h = 1.40$, $f' = 0.175$	$h = 1.44$, $f' = 0.20$
277.3	1.01	1.01	1.02 [b]	1.07 [b]
263.8	0.87	0.87	1.22	1.26
253.0	1.28	1.15	2.05	2.25
243.1	2.78	2.09	2.60	2.70
233.9	1.11	1.11	1.19	1.13
225.4	0.88	0.88	0.93	0.89
206.6	1.04	1.03	1.09	1.06
177.1	0.94	0.94	0.94 [b]	0.94 [b]
155.0	1.12	1.12	1.13	1.16
137.7 [c]	1.02	1.01	1.02	1.02
124.0 [c]	0.94	0.95	1.01	1.07
99.2 [c]	1.11	1.10	1.17	1.17

[a] All fits had about 120 degrees of freedom.
[b] Used to determine parameters of semiempirical models.
[c] Intensity of second order line fit as additional free parameter.

fit values for h also show no significant shift across the argon L-edge. The fit values for h, excluding those determined from the pulse height distributions just below and just above the argon L-edge, are consistent with a constant value of 1.42, which is itself within the uncertainties in the value of 1.41 ± 0.02 which we had obtained from the literature [18]. The χ^2_ν values are virtually identical for fits which fix h at 1.41 and fits which allow h to vary freely. The formal uncertainties in our best fit gas gain values are $\sim \pm 0.3\%$ while the 1σ variation within the set of fit gas gains is $\pm 0.9\%$ (excluding results for the two pulse height spectra that bracket the argon L-edge). This variation in the fit gas gains is consistent with the estimated accuracy of our gain normalization procedure, but we cannot rule out systematic errors of this magnitude in our model of the mean charge production.

The model predicts a 36.1 eV discontinuity in mean pulse height at the argon L-edge, which is in satisfactory agreement with our observations. According to the calculations, 14.6 eV of this is due to photoionization effects and the balance is produced by the sudden increase in secondary electron losses to the window due to the decreased absorption depth on the high energy side of the edge. Others have proposed that this drop in pulse height is due to incomplete secondary electron collection caused by a weak field region in close proximity to the presumably rough window surface. It seemed to us that a good test of the reality of our model would be to determine experimentally the division of the effect among these three possibilities.

The possibility of a weak field region near the window is easily tested by reducing the operating pressure, since both photoionization effects and the ratio of photon mean free path to the back-diffusion scale length are approximately independent of density. Reducing the pressure by 60% had no effect on the discontinuity, so field geometry near the window does not seem to contribute significantly.

Photoionization and electron diffusion effects were separated by replacing increasing portions of the argon in the gas mixture with helium. This left the diffusion scale length nearly the same while the small photoelectric cross section of helium increased the photon mean free path. Since essentially all of the X-rays were still absorbed by argon atoms, photoionization processes were unaffected. The result was that 12.4 ± 4 eV of the discontinuity persists when extrapolated to infinite absorption depth and is therefore attributable to changes in the photoionization processes in going across the edge. This is in reasonable agreement with the 14.6 eV predicted by the model.

5. Empirical models for other gasses

For most proportional counter gasses it would be impractical, if not impossible, to develop a model as detailed as our model for argon [2]. The necessary atomic data are not available. Examination of the detailed model, however, makes it possible to describe a simple semiempirical procedure which is a good approximation to the detailed model for argon over a wide range of energies. It will also be a good approximation for other gasses if the relative magnitudes of the major effects are similar to those for argon. The predicted response is described by a small number of free parameters. Some of these parameters change value at atomic absorption edges, but all required values can be inferred from a few properly chosen calibration lines.

The detailed model already makes use of analytic expressions that approximate the charge distributions resulting from secondary ionization, diffusion losses, and the electron avalanche. We discuss below a simple expression which approximates the net results of photoionization plus secondary ionization. In combination with the analytic descriptions of diffusion loss and the avalanche, this expression can be used to approximate the entire proportional counter response over a wide range of energies.

We discuss this approximation to the results of photoionization and secondary ionization in section 5.1. In section 5.2 we describe the algorithm for predicting proportional counter response, given values for the parameters, and in section 5.3 we describe a method to determine all of the necessary parameters from calibration data.

5.1. Approximations to the secondary electron distribution

An intermediate result from the detailed model for argon predicts the probability distribution of the total number of electrons produced following absorption of monoenergetic photons [2]. This is the secondary electron distribution after thermalization of all energetic electrons produced in the photoelectric absorption event, but prior to accounting for diffusion losses to the window. We find that this distribution can always be approximated rather well by a single Gaussian, despite the fact that it is the sum of single electrons plus Gaussians (which are themselves approximations to the ionization distribution produced by individual energetic electrons), averaged over all photoionization branches. Even for photon energies above the argon L-edge, where M- and L-shell photoionizations are both significant and contribute different mean numbers of electrons to the total secondary electron distribution, the gaussian never differs from the detailed model by more than 1.5% of the peak value. It thus makes sense to approximate the net results of photo- and secondary ionization with Gaussians, bypassing all the complexities of the photoionization process. It is of course necessary to be able to predict reliably the mean and width of these as functions of photon energy.

Although photoionization is the most complicated part of the detailed model, the net effect is primarily just a discontinuity in the mean number of total secondary electrons produced as the photon energy crosses an absorption edge. The detailed model approximates the probability of shake-up and shake-off processes (when energetically allowed) as constant between adjacent absorption edges. While this is certainly not exact, it appears to be an adequate approximation for argon, based on the good agreement with our P-10 counter data. This assumption of constant probabilities causes the prediction of the mean number of secondary electrons to increase linearly with photon energy, except in the small region just above each absorption edge where the initial photoelectron has so little kinetic energy that it is below the threshold for shake-up, shake-off, or secondary ionization. This is the only nonlinearity which has been taken into account in the detailed model.

Ignoring this, we can approximate the mean number of secondary electrons by

$$\langle N(E_\gamma)\rangle = \frac{E_\gamma - \Delta E_k}{W}, \tag{4}$$

where the energy offset ΔE_k is different for each energy interval k between adjacent atomic absorption edges and W, the average amount of energy required for each additional ionization, is just the asymptotic value of $W(E)$ described in section 2.2.

This approximation introduces a substantial error just above an edge, but the effect is limited to a small energy interval where even the detailed model is probably inaccurate, as none of the effects of fine structure in the absorption cross sections near the edge have been taken into account.

We examined the energy dependence of the width of the secondary electron distribution in terms of an effective Fano factor,

$$f' \equiv \frac{\sigma^2(E_\gamma)}{(\langle N(E_\gamma)\rangle - 1)}. \tag{5}$$

Fig. 8 shows f' as a function of photon energy E_γ, where $\langle N(E_\gamma)\rangle$ and $\sigma^2(E_\gamma)$ are derived from secondary electron distributions predicted by the detailed model. We would recover the Fano factor, f, exactly if the initial energy were the kinetic energy of a single electron. We include model calculations for photon energies beyond the range of our data to show the model behavior as the energy of photoelectrons from the L-shell becomes large. For photon energies above a few hundred eV, the effective Fano factor is nearly equal to the Fano factor for a single electron with the same energy. Most of the slope of f' vs E_γ in fig. 8 is due to the energy-dependent Fano factor used in the detailed models [2]. The small jump in f' at the argon L-edge is due to the increased number of branching possibilities for photon energies above the edge.

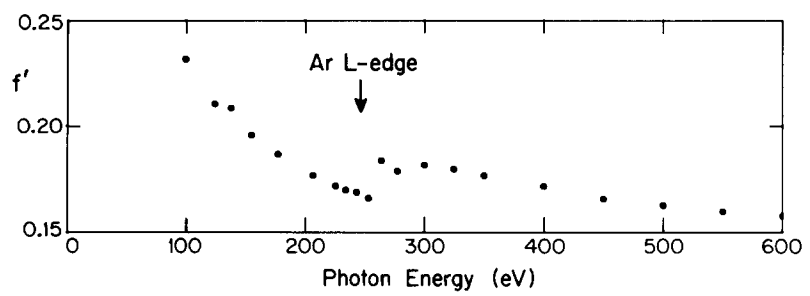

Fig. 8. The dispersion of the net secondary electron distribution calculated from the detailed model prior to including electron loss to the window, as a function of E_γ. The calculated dispersion has been divided by the mean number of electrons minus one to give an "effective Fano factor" $f'(E_\gamma) \equiv \sigma^2(E_\gamma)/(\langle N(E_\gamma)\rangle - 1)$.

Approximating f' as a constant will introduce only small errors in the predicted width of the total response of conventional proportional counters, since the width of the response is dominated by avalanche statistics. For gas scintillation counters, or other variants which eliminate or reduce the effects of the avalanche, fig. 8 indicates that the error in the width of the response (which is dominated by f' in the absence of avalanche statistics) would be as large as 25% if f' were treated as a constant. In such cases it appears more than adequate (for argon, at least) to approximate f' by a linear function with different slope and intercept values in each interval between absorption edges.

Given this Gaussian approximation to the secondary electron distribution, we can proceed using the same analytic expressions as the detailed model to describe diffusion losses and the electron avalanche. The only difference is that the ratio of diffusion coefficient to drift velocity, D/w, the Polya parameter, h, and the gas gain, μ, are treated as free parameters and are determined by fits to calibration data.

5.2. The semiempirical pulse height distribution

Within the limits of the approximations discussed above, we can estimate the response of a proportional counter to monochromatic X-rays of energy E_γ given the W value, the energy offsets ΔE_k, the effective Fano factor f', the ratio of diffusion coefficient to drift velocity D/w, the mean absorption depth λ, the gas gain μ, and the avalanche width parameter h. In this section we show how to calculate the proportional counter response given values for all parameters. Section 5.3 will describe how empirical values for these parameters can be derived from a limited number of calibration lines.

The average number of secondary electrons $\langle N(E_\gamma)\rangle$ is given by eq. (4) where ΔE_k is chosen for the interval between adjacent absorption edges which includes E_γ. The relative probability $Q''(i)$ of producing exactly i secondary electrons is estimated from the Gaussian distribution function

$$Q''(i) = \exp\left(\frac{-\left(i - \langle N(E_\gamma)\rangle\right)^2}{2f'\left(\langle N(E_\gamma)\rangle - 1\right)}\right), \tag{6}$$

where we have taken the width from eq. (5), and the normalized probability $Q'(i)$ is given by

$$Q'(i) = \frac{Q''(i)}{\sum_{j\geq 1} Q''(j)}; \quad i > 0,$$

$$= 0; \qquad i \leqq 0. \tag{7}$$

This is slightly different from a true Gaussian as it is only evaluated for integer numbers of electrons and is truncated for values less than or equal to zero.

Diffusion losses to the window are calculated exactly as in the detailed model. The distribution of number of electrons lost to diffusion in the model of Inoue et al. [9] depends only on the dimensionless parameter $\kappa \equiv D/w\lambda$ where D is the diffusion coefficient, w the drift velocity, and λ the mean absorption depth. Jahoda and McCammon [2] show that for $\kappa < 1$ (in our counter κ was less than 0.13 for all energies considered), the probability $f(n, N_0)$ that exactly n electrons reach the avalanche region from a cloud of N_0 electrons produced by an individual X-ray absorbed in the counter can be approximated by

$$f(n, N_0) = \kappa\left(1 - \frac{n}{N_0}\right)^{(\kappa-1)} \frac{1}{N_0}. \tag{8}$$

Combining this result with the initial secondary electron distribution $Q'(i)$ gives the probability $Q(i)$ that exactly i electrons reach the avalanche region. Using the above expression for $f(n, N_0)$, $Q(i)$ is given by

$$Q(i) = Q'(i) - \sum_{m=0}^{i-1}\left(Q'(i)\kappa\left(1 - \frac{m}{i}\right)^{(\kappa-1)}\frac{1}{i}\right)$$

$$+ \sum_{n>i}\left(Q'(n)\kappa\left(1 - \frac{i}{n}\right)^{(\kappa-1)}\frac{1}{n}\right). \tag{9}$$

The terms in this equation are the probability of producing exactly i electrons minus the probability of losing one or more electrons given an initial production of i electrons plus the probability of initially producing more than i initial electrons and losing all but i of them. While the individual corrections are small for argon, the cumulative effect on the shape of the distribution is large (see fig. 4).

The distribution $Q(i)$ for any E_γ can be determined from eqs. (4)–(9), given values for W, f', D/w, λ, and the appropriate ΔE_k. The output pulse height distribution can then be determined by convolving $Q(i)$ with the avalanche distribution function, as shown in eqs. (2) and (3). This last step requires values for μ and h.

5.3. Determining the parameters

The model requires values for the parameters W, ΔE_k, f', D/w, λ, μ and h. The value for W is constant and need not be precisely known. Its effect on the predicted mean pulse height enters only as μ/W while its effects on the width of the secondary electron distribution scale very nearly as f'/W. For most gas mixtures W is between 25 and 33 eV, and simply assuming a value of 29 eV will be accurate enough. (W can be as low as 15 eV in Penning mixtures, and more care must be taken in such cases.) The fit values for μ and f' will compensate for inaccuracies in W.

The mean absorption depth λ is easily calculated from the gas composition and atomic absorption cross sections as given, for example, in ref. [19]. The parame-

ters D/w, μ, and h are independent of E_γ, so a single value needs to be determined for each by fitting to calibration lines. The energy offsets ΔE_k are constant between atomic absorption edges but have distinct values on either side of each absorption edge. Therefore, if there are n absorption edges in the photon energy range of interest, $n+1$ values of ΔE_k must be determined. The effective Fano factor f' may be treated as a constant over the entire energy range of interest in conventional counters. In counters with reduced or no avalanche broadening, f' should be approximated as a linear function of photon energy, with discontinuities in both slope and intercept at absorption edges as discussed in section 5.1.

It is necessary to determine the energy offsets in eq. (4) separately in each interval between atomic absorption edges of the counter gas. Therefore, at least one calibration line is required in each interval. Each calibration line should be well above the next lower absorption edge, and thus out of the small region just above an absorption edge where eq. (4) is a poor approximation to the mean number of secondary electrons. One additional calibration line is necessary to determine the apparent gas gain. This can be either a line at high enough energy that $E_\gamma \gg \Delta E_k$ (though care must be taken that gain saturation is not a problem) or a second line in one of the energy intervals between adjacent absorption edges. In the latter case the second line should be separated in energy from the first by as much as practical. This set of calibration lines will also suffice to determine f', D/w, and h for conventional proportional counters. For counters with reduced or no avalanche effects a second line is needed in each interval between absorption edges in order to approximate the effective Fano factor as a function of energy.

It is impractical to try to determine all of the parameters simultaneously as several are strongly coupled. The predicted mean pulse height is a strong function of both the offset ΔE_k and the mean gas gain μ. The width of the pulse height distribution is a function of both the Polya parameter h and the effective Fano factor f'. In this section we describe an iterative method for determining the parameters one at a time. At each step the data from a calibration line are fit using the algorithm of section 5.2, allowing only a subset of the parameters to vary. Our general approach is to first determine the apparent gas gain, followed by those parameters which affect the shape of the distribution, and finally the offsets ΔE_k. This is only one example of a workable procedure and other approaches could be used as appropriate to the precision of the available calibration spectra and the required accuracy of the model.

To determine the apparent gas gain μ from a single high energy line, the response function (section 5.2) can be fit with the gas gain μ and the avalanche width parameter h as free parameters. Values for ΔE_k (which is $\ll E_\gamma$) and D/w are fixed at zero. The average energy required per secondary electron W and the effective Fano factor f' are also fixed (29 eV and 0.2 are reasonable estimates if no data are available).

Once the gas gain has been estimated, a better estimate of h may be obtained in some cases by fitting a lower energy calibration line which still has a relatively large mean absorption depth and consequently is little affected by diffusion. The response function is fit with ΔE_{k_1} and h as free parameters, μ fixed at the value determined above, W and f' fixed at the same values used above, and D/w set equal to zero. The calibration line with the smallest mean absorption depth can now be used to fit the ratio D/w. The response function is fit with D/w and ΔE_{k_2} as free parameters, and values for h, μ, W, and f' as used or determined above. The resulting best fit value of D/w may be used to redetermine h at an energy where diffusion losses are less important. If the calibration data have good statistical precision, a set of fits with f' fixed at different values may be performed; the series which converges to the smallest χ^2 provides the best estimate of f'.

If the calibration data are not of sufficient quality to determine both h and f', the effective Fano factor may be fixed and the best fit value of h will compensate for errors in the total width of the detector response introduced by inaccurate f' values. This is not an exact correction as f' and h produce different skewness and higher moments in the predicted pulse height distribution. For the data in fig. 6, however, the quality of the fits is not strongly affected if f' is fixed at values $\pm 20\%$ of its nominal value. (The χ^2 increases by about 5 for two free parameters and 120 degrees of freedom while best fit values for h vary from 1.1 to 1.9.) A value of 0.20 for the effective Fano factor is probably accurate to $\pm 20\%$ for most non-Penning gas mixtures, although it can be as small as 0.05 for Penning mixtures [16]. With good calibration data f' can be determined empirically.

The process may be iterated until stable values of D/w, h, and f' are found. Because diffusion affects primarily the shape of the low pulse height tail, the value of D/w is relatively independent of h and f'. However, it can have a large effect on ΔE_k for lines with very small absorption depths. The initial estimate of the gain can be checked by repeating the fits which determined μ, but with D/w, h, and f' fixed at the best fit values. The entire procedure can be iterated as often as necessary, although stable values of D/w, h, and f' are usually determined in one or two iterations. With the resulting f', D/w, h, and μ, one last fit to each calibration line is required to establish the final values of the offsets ΔE_k.

Columns 4 and 5 of table 1 give the χ^2_ν values for two applications of this procedure to our synchrotron

source data. In both cases we determined all parameters except gain from the pulse height spectra of 177 and 277 eV photons. We took values for the gas gain from the detailed fits in order that the difference in χ^2_ν values between the detailed models and the semiempirical approximation would reflect only differences in the shape of the predicted response. (With more usual laboratory facilities, we could have used the easily-produced boron, carbon, and aluminum K_α fluorescent lines at 183, 277, and 1490 eV to determine all parameters including gain.) For both sets we took $W = 28.5$ eV. Column 4 represents fits where f' and h were both adjusted to give the best fit (the final values were $f' = 0.175$ and $h = 1.40$), while column 5 gives the results when f' was fixed at 0.20 (the best fit for h was 1.44). The χ^2_ν values obtained from the semiempirical predictions are a significant improvement over the Poisson and Prescott fitting functions and the number of free parameters required is reduced.

Acknowledgements

It is a pleasure to thank J. Lenz, J. Morrison, and K. Wosilait for their help in making the measurements, M.A. Prasad for providing unpublished data, and M. Inokuti and W. Neumann for helpful discussions. We appreciate the assistance of B. Cole and C. Pruett in setting up the monochromator on the University of Wisconsin Tantalus II synchrotron light source. This research was supported in part by the National Aeronautics and Space Administration under grant NAG 5-629.

References

[1] F.R. Harndon Jr., D.G. Fabricant, D.E. Harris and J. Schwartz, Smithsonian Astrophysical Observatory Special Report 393 (1984).
[2] K. Jahoda and D. McCammon, Wisconsin Astrophysics 256, Proportional Counters as Low Energy Photon Detectors (1987).
[3] D. Combecher, Radiat. Res. 84 (1980) 189.
[4] M. Inokuti, Radiat. Res. 64 (1975) 6.
[5] G.D. Alkhazov, Sov. Phys. - Techn. Phys. 16 (1972) 1540.
[6] K. Unnikrishnan and M.A. Prasad, Radiat. Res. 80 (1979) 225.
[7] M. Kase, J. Kikuchi and T. Doke, Nucl. Instr. and Meth. 163 (1979) 289.
[8] M.A. Prasad, private communication.
[9] H. Inoue, K. Koyama, M. Matsuoka, T. Ohashi and Y. Tanaka, Nucl. Instr. and Meth. 157 (1978) 295.
[10] G.D. Alkhazov, Nucl. Instr. and Meth. 89 (1970) 155.
[11] S.C. Curran, A.L. Cockroft and J. Angus, Phil. Mag. 40 (1949) 929.
[12] W. Neumann, 7th Symp. on Microdosimetry, Comm. Eur. Communities [Rep.] EUR 7147 (1981) p. 1067.
[13] P.J. Campion, Nucl. Instr. and Meth. 112 (1973) 75.
[14] A.J.P.L. Policarpo, Space Sci. Instr. 3 (1977) 77.
[15] O.H.W. Siegmund, S. Clothier, J.L. Culhane and I.M. Mason, IEEE Trans. Nucl. Sci. NS-30 (1982) 350.
[16] H. Sipilä, IEEE Trans. Nucl. Sci. NS-26 (1979) 181.
[17] H.E. Schwartz and I.M. Mason, Nature 309 (1984) 532.
[18] G.D. Alkhazov, Nucl. Instr. and Meth. 75 (1969) 161.
[19] B.H. Henke, P. Lee, T.J. Tanaka, R.L. Shimabukuro and B.K. Fujikawa, At. Data Nucl. Data Tables 27 (1982) 1.